PCCP

PAPER

View Article Online
View Journal

Cite this: DOI: 10.1039/c6cp05756j

Oxygen diffusion and surface exchange in the mixed conducting oxides $SrTi_{1-y}Fe_yO_{3-\delta}$†

Veronika Metlenko,[a] WooChul Jung,‡[b] Sean R. Bishop,[b] Harry L. Tuller[bc] and Roger A. De Souza*[a]

Received 19th August 2016,
Accepted 8th October 2016

DOI: 10.1039/c6cp05756j

www.rsc.org/pccp

Oxygen transport in the mixed ionic–electronic conducting perovskite-oxides $SrTi_{1-y}Fe_yO_{3-\delta}$ (with y = 0.5 and y = 1.0) was studied by oxygen isotope exchange measurements. Experiments were performed on thin-film samples that were grown by Pulsed Laser Deposition (PLD) on MgO substrates. Isotope penetration profiles were introduced by $^{18}O_2/^{16}O_2$ exchanges into the plane of the films at various temperatures in the range $773 < T/K < 973$ at an oxygen activity aO_2 = 0.5. Isotope profiles were determined subsequently by Time-of-Flight Secondary Ion Mass Spectrometry (ToF-SIMS), and their analysis yielded tracer diffusion coefficients D^* and oxygen surface exchange coefficients k^*. Activation energies for oxygen diffusion ΔH_{D^*} and surface exchange ΔH_{k^*} were obtained. Isothermal values of D^* and values of ΔH_{D^*} are compared with literature data as a function of Fe content. D^* is seen to increase monotonically with Fe content; ΔH_{D^*} shows more complex behaviour. D^* and ΔH_{D^*} are also compared with the predictions of defect-chemical models. Analogous comparisons with literature data for k^* and ΔH_{k^*} indicate, in contrast to prior studies, no mechanistic difference between electron-poor and electron-rich materials. It is concluded that the single operative mechanism of surface exchange for the entire series of STF compositions requires conduction-band electrons (minority electronic charge-carriers).

1 Introduction

A fundamental understanding of mass transport processes in a mixed ionic-electronic conductor (MIEC) is a prerequisite for the efficient selection and optimisation of such materials. In the case of oxygen-ion conducting MIECs that find application as SOFC cathodes and oxygen permeation membranes, the two key transport processes are the diffusion of oxygen in the bulk and the incorporation of oxygen at the surface. These processes are characterised by an oxygen diffusion coefficient D, and a surface exchange coefficient k.[1–9]

Real MIEC materials are often chemically complex systems. The best oxygen-ion MIEC, $(Ba,Sr)(Co,Fe)O_{3-\delta}$,[10–13] for example, displays complex defect behaviour and, in the temperature range of interest, a phase decomposition.[14–17] Such complexities make the acquisition of fundamental knowledge regarding such transport processes far from simple. Indeed, much progress has been made by studying model systems, that is, systems that are sufficiently simple, chemically and structurally, but still sufficiently close to real MIEC materials that the essential chemical behaviour is captured.

$SrTiO_3$ has long been considered an ideal MIEC oxide,[18] and many studies have been devoted to elucidating mass transport processes within it. Oxygen diffusion in the bulk is well understood: the mechanism is known (the migration of oxygen vacancies), and the various oxygen diffusion coefficients (tracer, chemical, conductivity)[6] can be predicted quantitatively as a function of thermodynamic control parameters (temperature, oxygen activity and dopant concentration), even taking complicating trapping effects into account.[19–33] The same cannot be said, however, of the surface process. Despite extensive studies,[30,34–41] there is no concensus regarding the mechanism of oxygen surface exchange, and analytical expressions for the surface exchange coefficients that predict the dependence on thermodynamic control parameters are still lacking.

Not only is $SrTiO_3$ a model system, it is also the basis of a further, newer model system: $SrTi_{1-y}Fe_yO_{3-\delta}$ (STF). Such materials form a continuous solid solution over the entire compositional range ($0 < y < 1$),[42–44] and under oxidising conditions, exhibit simple cubic perovskite symmetry. Under reducing conditions, and depending on the temperature,[45] the end member $SrFeO_{2.5}$ has ordered vacancies, forming brownmillerite $Sr_2Fe_2O_5$. In a sense,

[a] Institute of Physical Chemistry, RWTH Aachen University, 52056 Aachen, Germany. E-mail: desouza@pc.rwth-aachen.de; Fax: +49 241 80 92129; Tel: +49 241 80 94739
[b] Department of Materials Science and Engineering, Massachusetts Institute of Technology, Cambridge, MA 02139, USA
[c] International Institute of Carbon Neutral Energy Research, Kyushu University, Fukuoka 819-0395, Japan

† Dedicated to Prof. Rainer Waser on the occasion of his 60th birthday.

‡ Present address: Department of Materials Science and Engineering, Korea Advanced Institute of Science and Technology (KAIST), Republic of Korea.

the STF oxides constitute a superior model system, as they exhibit excellent electrochemical performance and may be used as actual SOFC cathodes.[46,47]

There are only a few studies that have examined oxygen-ion transport[43,44,48–55] and surface exchange,[37,46,47,51,54,56–59] and these are distributed over the whole STF compositional range. Again, there is no concensus regarding the mechanism(s) of surface exchange.

In this study we examine oxygen transport in two STF compositions, $SrTi_{0.5}Fe_{0.5}O_{3-\delta}$ (STF50) and $SrFeO_{3-\delta}$ (SF), using isotope exchange and subsequent determination of the isotope profile in the solid by Time-of-flight Secondary Ion Mass Spectrometry (ToF-SIMS).[60–63] This method allows an unambiguous, simultaneous determination of both the oxygen tracer diffusion coefficient, D^*, and the surface exchange coefficient, k^*. Compositions were investigated in the form of thin films, as we experienced difficulties in obtaining ceramic samples of sufficiently high density. Having obtained transport data, we consider, together with literature data, the variations in D^* and k^* as a function of Fe concentration, from dilute levels of Fe in $SrTiO_3$ all the way up to $SrFeO_{3-\delta}$.

2 Defect chemistry of $SrTi_{1-y}Fe_yO_{3-\delta}$

In order to interpret measured tracer diffusion coefficients, one requires the concentrations of the oxygen defects that are responsible for diffusion. To this end, we describe, in the following, three different defect-chemical descriptions of $SrTi_{1y}Fe_yO_{3-\delta}$: Model I considers Fe in $SrTiO_3$ as a dilute solution, and applies thus to compositions with Fe site fractions $y < 0.01$; Model II treats the STF solid solutions ($0 < y < 1$) as pseudo-brownmillerites (*i.e.*, as systems with ordered vacancies); and Model III treats the STF solid solutions as perovskites with randomly distributed vacancies. A further variant, which is not employed here, would be the inherently-deficient-sublattice approach of Norby.[64,65]

2.1 Model I: Fe-doped $SrTiO_3$

The defect chemical model for weakly acceptor-doped $SrTiO_3$ is well established.[66–77] The electroneutrality condition in the temperature range of interest and under dry conditions (such that the concentration of interstitial protons $H_i^\bullet$ can be ignored) can be written as

$$[e'] + [Fe'_{Ti}] = [h^\bullet] + 2[V_O^{\bullet\bullet}] \quad (1)$$

These defect concentrations are interrelated *via* equilibrium defect chemical reactions, and there are three relevant reactions:

(i) The generation of electrons and holes by thermal excitation across the band gap,

$$\text{null} \rightleftharpoons h^\bullet + e', \quad (2)$$

with equilibrium constant,

$$[e'][h^\bullet] = K_{eh}(T) = K_{eh}^\circ \exp\left(-\frac{E_{bg}(T)}{k_B T}\right). \quad (3)$$

$E_{bg}(T)$ is the temperature-dependent bandgap.

(ii) The reduction of the oxide

$$O_O^\times \rightleftharpoons \frac{1}{2}O_2(g) + V_O^{\bullet\bullet} + 2e'. \quad (4)$$

The equilibrium constant of this reaction is given by

$$\frac{[V_O^{\bullet\bullet}][e']^2 aO_2^{1/2}}{[O_O^\times]} = K_{red}(T) = K_{red}^\circ \exp\left(\frac{-\Delta H_{red}}{k_B T}\right). \quad (5)$$

with reduction enthalpy ΔH_{red}.

(iii) The ionisation reaction of the Fe acceptor cation

$$Fe_{Ti}^\times \rightleftharpoons Fe'_{Ti} + h^\bullet, \quad (6)$$

with equilibrium constant

$$\frac{[Fe'_{Ti}][h^\bullet]}{[Fe_{Ti}^\times]} = K_{ion}(T) = K_{ion}^\circ \exp\left(\frac{-\Delta H_{ion}(T)}{k_B T}\right). \quad (7)$$

$\Delta H_{ion}(T)$ is the temperature-dependent enthalpy of dopant ionisation. The total amount of dopant present in the system is thus divided into charged and neutral dopants,

$$[Fe_{Ti}] = [Fe'_{Ti}] + [Fe_{Ti}^\times]. \quad (8)$$

Solving eqn (1), (3), (5), (7) and (8) simultaneously allows the prediction of the five defect concentrations. In this study we used the internally consistent set of equilibrium constants derived by Denk *et al.*[73] These values, it is emphasised, do not vary with Fe content, as Fe is considered as a dilute dopant.

The tracer diffusion coefficient of oxygen in a cubic perovskite with a dilute concentration of oxygen vacancies can be written as

$$D^* = f_V^* D_V n_V, \quad (9)$$

with $f_V^* = 0.69$.[78] The contribution to D^* from oxygen interstitials can be reasonably neglected, as the concentration of these defects is predicted to be extremely small in weakly acceptor-doped $SrTiO_3$: $[O_i''] \propto [V_O^{\bullet\bullet}]^{-1} \exp(\Delta H_{aF}/k_B T)$, with the enthalpy of anti-Frenkel disorder, according to theoretical estimates,[79,80] being $\Delta H_{aF} \approx$ 7–8 eV.

From eqn (9) one can show[30] that the measured enthalpy of tracer diffusion can be expressed as

$$\Delta H_{D^*} = \Delta H_{mig,V} + \Delta H_{gen,V}, \quad (10)$$

where $\Delta H_{mig,V}$ is the activation enthalpy of oxygen-vacancy migration, and $\Delta H_{gen,V}$ is the generation enthalpy of oxygen vacancies, which describes the change in vacancy concentration with temperature:

$$\Delta H_{gen,V} = -k_B \left(\frac{\partial \ln[V_O^{\bullet\bullet}]}{\partial(1/T)}\right)_{aO_2}. \quad (11)$$

If Fe were only present as Fe^{3+} and solely compensated by oxygen vacancies at all temperatures, that is, $[Fe'_{Ti}] = 2[V_O^{\bullet\bullet}]$, then $\Delta H_{gen,V}$ is exactly zero.

2.2 Model II: $SrTi_{1-y}Fe_yO_{3-\delta}$ solid solutions

In order to define point defects, one has to specify an ideal (reference) structure. In the case of the STF solid solutions, one could use either acceptor-doped $SrTiO_3$ or donor-doped $SrFeO_{2.5}$ as reference states but only up to the respective limits of dilute solutions. A description of STF50, say, based on either of these end-members will, therefore, be inadequate. Rothschild *et al.*[49] solved this problem by considering each $SrTi_{1-y}Fe_yO_{3-y/2}$ composition as a separate reference structure. Thus the amount y of Fe and the amount $y/2$ of oxygen vacancies per formula unit refer to the reference structure and do not count as defects. In essence, each STF composition is a pseudo-brownmillerite. This approach, it is emphasised, is able to describe the electrical conductivity of the STF oxides as a function of Fe content, temperature and oxygen activity extremely well.

In each pseudo-brownmillerite system, oxygen ions can be excited by anti-Frenkel disorder from their regular lattice sites into the vacant oxygen-ion sites of the structure,

$$O_O^\times + V_i^\times \rightleftharpoons V_O^{\bullet\bullet} + O_i'' ; \tag{12}$$

the equilibrium constant for this anti-Frenkel reaction is

$$\frac{[O_i''][V_O^{\bullet\bullet}]}{[V_i^\times][O_O^\times]} = K_{aF}(T,y) = K_{aF}^\circ(y)\exp\left(\frac{-\Delta H_{aF}}{k_B T}\right) \tag{13}$$

The two further reactions of importance—electron–hole generation and reduction of the oxide—are the same as in Model I, but here, the equilibrium constants of these reactions are a function of both temperature and Fe content, namely,

$$[e'][h^\bullet] = K_{eh}(T,y) = K_{eh}^\circ(T)\exp\left(-\frac{E_{bg}(T,y)}{k_B T}\right) \tag{14}$$

and

$$\frac{[V_O^{\bullet\bullet}][e']^2 aO_2^{1/2}}{[O_O^\times]} = K_{red}(T,y) = K_{red}^\circ(y)\exp\left(\frac{-\Delta H_{red}(y)}{k_B T}\right). \tag{15}$$

The electroneutrality condition for Model II reads, therefore,

$$[e'] + 2[O_i''] = [h^\bullet] + 2[V_O^{\bullet\bullet}]. \tag{16}$$

(Fe is part of the structure and hence does not appear in the electroneutrality condition). The four defect concentrations are found by solving eqn (13)–(16). The numerical values of the equilibrium constants were taken from Rothschild *et al.*[49]

At first sight it appears from the discussion above that there are two ionic charge carriers, $V_O^{\bullet\bullet}$ and O_i'', which may contribute to oxygen diffusion. In such a case, the measured tracer diffusion coefficient can be expressed as the sum of the two contributions,

$$D^* = f_V^* D_V \frac{[V_O^{\bullet\bullet}]}{[O_O^\times]} + f_i^* D_i \frac{[O_i'']}{[O_O^\times]}, \tag{17}$$

where $f_{V,i}^*$ are the tracer correlation factors of oxygen vacancies (V) and oxygen interstitials (i); $D_{V,i}$ are the diffusion coefficients of these defects; and $[V_O^{\bullet\bullet}]$, $[O_i'']$ and $[O_O^\times]$, the concentrations of oxygen vacancies, oxygen interstitials and regular oxygen ions. In order to interpret measured values of D^*, we require independent knowledge of both D_V and D_i (for given $f_{V,i}^*$ and $[V_O^{\bullet\bullet}]$, $[O_i'']$ and $[O_O^\times]$). A closer examination of the problem reveals, however, that the contribution from oxygen interstitials is zero. This is because there is no connected migration pathway for O_i'' in a (pseudo-)brownmillerite. That is, an oxygen ion sitting in a structural vacancy cannot migrate directly to an empty structural vacancy. The tracer diffusivity is thus given by eqn (9), if we assume that f_V^* is not changed vastly from its value for the dilute regime (f_V^* could, conceivably, be a function of vacancy concentration and thus vary with T and y.) The concentration of vacancies is the value relative to $3 - y/2$, and the partial differential operator of eqn (11) acts at constant aO_2 and y.

2.3 Model III: $SrTi_{1-y}Fe_yO_{3-\delta}$ solid solutions

If the oxygen vacancies are not ordered in an STF composition, then it is the deviation from $SrTi_{1-y}Fe_yO_3$, rather than the deviation from $SrTi_{1-y}Fe_yO_{3-y/2}$, that counts. In this model, we have simply taken, therefore, the values of $\delta(T,aO_2,y)$ determined by thermogravimetric analysis reported in the literature.[45,81]

The tracer diffusion coefficients are assumed to be given by eqn (9) with $f_V^* = 0.69$, even though the concentration of vacancies is well beyond the dilute limit.

2.4 Summary of defect-chemical results

Before we consider the predictions of the three models, we note that, in all of three models described above, defect interactions involving oxygen vacancies (either with each other or with Fe species) are not taken into account. We return to this issue in Section 5.1.

Fig. 1(a) shows the variation in the vacancy concentration with Fe content at $T = 873$ K for the three models. Note that the vacancy concentration is relative to $Sr(Ti,Fe)O_3$ for Models I and III but relative to $SrTi_{1-y}Fe_yO_{3-y/2}$ for Model II. Also included is the theoretical variation in oxygen-vacancy concentration if Fe was all present as Fe^{3+}. Considered together, the data suggests (i) that, at low [Fe], most of the Fe is present as Fe^{3+} but with a significant amount of Fe^{4+}; and (ii) that at much higher [Fe], the proportion of Fe^{3+} increases (since the symbols approach the dotted line).

The corresponding variation in the generation enthalpy is plotted in Fig. 1(b). In general, the values are very low, with $\Delta H_{gen,V} < 0.25$ eV. For other perovskite compositions, *e.g.*, $(La,Sr)(Mn,Co)O_{3-\delta}$,[82] $\Delta H_{gen,V}$ can approach 3 eV. Model I suggests a small increase in $\Delta H_{gen,V}$ over the regime of Model I's validity; Model II predicts a decrease in $\Delta H_{gen,V}$ and Model III constant behaviour, as y approaches unity, that is, towards $SrFeO_{3-\delta}$.

3 Experimental

Dense thin films of STF50 and SF were grown on (100)-oriented MgO substrates held at $T = 973$ K in an atmosphere of 10 mTorr

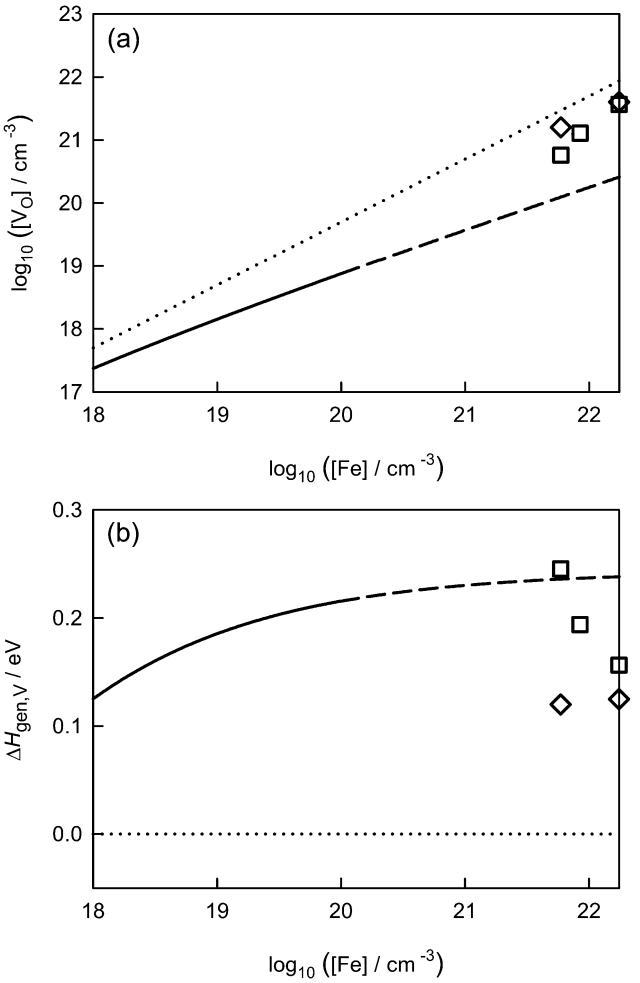

Fig. 1 (a) Concentration of oxygen vacancies, $[V_O^{\bullet\bullet}]$, as a function of Fe concentration, [Fe], in STF at T = 873 K predicted from the three point-defect models. (b) The generation enthalpy of oxygen vacancies, $\Delta H_{gen,V}$, [defined in eqn (11)] as a function of Fe concentration, [Fe], in STF. Solid black line, Model I (shown as a dashed line outside the realm of its validity).[73] Open squares, Model II.[49] Open diamonds, Model III.[45,81] The dotted lines in (a) and (b) refer to $[Fe] = 2[V_O^{\bullet\bullet}]$ (*i.e.* the assumption is that all Fe is present as Fe^{3+}).

O_2 by Pulsed Laser Deposition (PLD). Laser pulses of 400 mJ were employed at a repetition rate of 8 Hz. Deposited films exhibited thicknesses of *ca.* 500 nm for STF50 and *ca.* 250 nm for SF. X-ray diffraction patterns indicated single-phase perovskite with no significant preferred orientation. Images of the films' surfaces taken with Atomic Force Microscopy (AFM) indicated a grain size in the range of 50–100 nm and an r.m.s. surface roughness of 1.5 nm.

The samples were subsequently sputter-coated with gold (to a thickness of *ca.* 300 nm), and then annealed at T = 673 K for five hours in air to stabilise the gold layer. Finally, two trenches were cut into the samples, with a scalpel, so that isotope exchange could only take place within the trenches (see Fig. 2). In this way the labelled oxygen is constrained to diffuse in the plane of the film.[83] In particular, the use of MgO as a substrate simplifies the diffusion problem by strongly hindering isotope leakage out of the STF films.

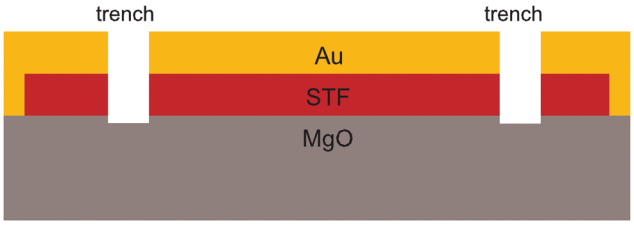

Fig. 2 Geometry of thin-film samples employed in this study for diffusion experiments. The two trenches were made with a scalpel.

A thin-film sample was first equilibrated, at the desired temperature and at an oxygen activity of $aO_2 = 0.5$, in molecular oxygen of normal isotopic abundance for a period of time ten times longer than that of the isotope anneal, $t_{eq} = 10t_{ex}$. It was then quenched to room temperature, after which it was annealed in a large volume of ^{18}O-enriched molecular oxygen at the same temperature and oxygen activity. Under these conditions—surface-limited kinetics of tracer incorporation from a large volume of gas into a semi-infinite medium[62]—the appropriate solution of the diffusion equation is[84]

$$\frac{n^*(x) - {n_{bg}}^*}{{n_g}^* - {n_{bg}}^*} = \mathrm{erfc}\left(\frac{x}{2\sqrt{D^* t_{ex}}}\right) - \exp\left(hx + h^2 D^* t_{ex}\right) \times \mathrm{erfc}\left(\frac{x}{2\sqrt{D^* t_{ex}}} + h\sqrt{D^* t_{ex}}\right) \quad (18)$$

where $n^*(x)$ is the measured isotope profile in the solid; and ${n_{bg}}^*$ and ${n_g}^*$ are the ^{18}O isotope fractions in the equilibration and isotope anneal gases respectively. D^* is the oxygen tracer diffusion coefficient; $h = k^*/D^*$, with k^* being the oxygen surface exchange coefficient.

Time-of-Flight Secondary Ion Mass Spectrometry (ToF-SIMS) measurements, on a TOF-SIMS IV (IONTOF, Münster, Germany), were used to determine the isotope profiles within the films. A high-current beam of 2 keV Cs^+ ions was rastered over an area of 700 μm × 700 μm, adjacent to a trench, in order to sputter etch, first, the Au layer off completely, and second, several nanometers of the STF film. Subsequently, a series of secondary ion images were obtained with a finely focussed beam of 25 keV Ga^+ ions, rastered over an area of 500 μm × 500 μm. Charge compensation was achieved with a high-intensity beam of low-energy electrons. The analysis was performed in burst mode,[28] and negative secondary ions were monitored.

${n_{bg}}^*$ and ${n_g}^*$ were determined by ToF-SIMS analysis of Si wafers that had been thermal oxidised in the respective gases: ${n_{bg}}^* = 0.002$ and ${n_g}^* = 0.93$.

4 Results

An example isotope profile is shown in Fig. 3. The experimental data are described well by eqn (18). For each sample, a number of profiles were obtained from various sites along the trenches. The corresponding average values of D^* and k^* are plotted in Fig. 4.

At all investigated temperatures, values of D^* for SF are consistently higher than for STF50 by a factor of roughly two.

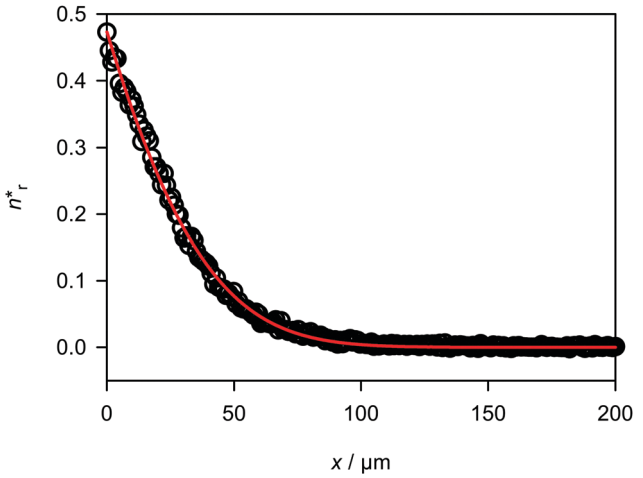

Fig. 3 Oxygen isotope profile obtained by ToF-SIMS analysis of an STF50 thin-film structure annealed at T = 873 K for $t_{ex} = 3.7 \times 10^3$ s at aO_2 = 0.5. Black circles refer to experimental data. The red line is the fit to eqn (18).

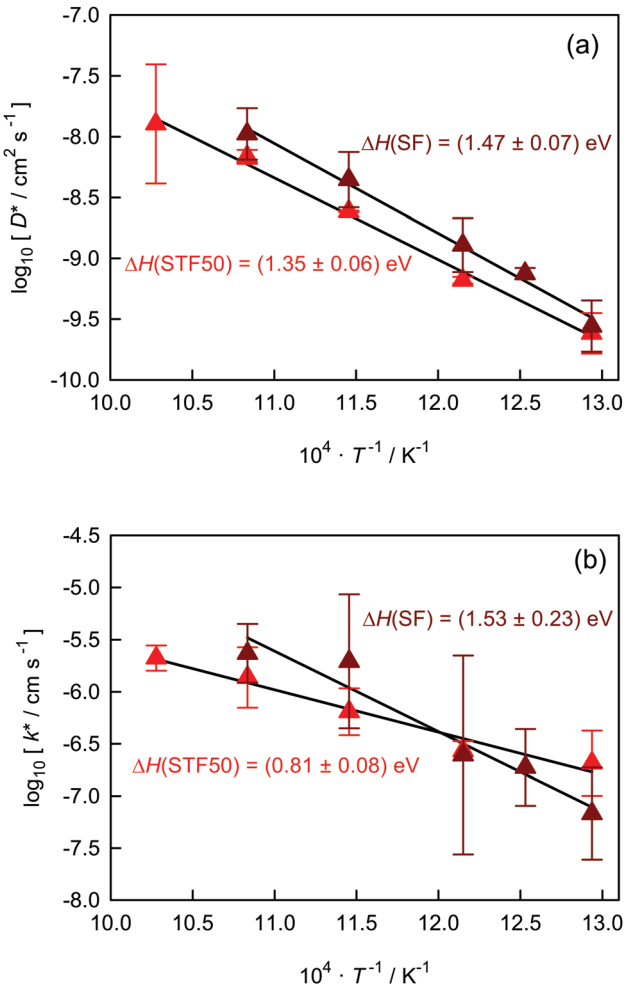

Fig. 4 Oxygen transport data obtained for STF50 and SF thin films at aO_2 = 0.5 as a function of inverse temperature: (a) oxygen tracer diffusion coefficients, (b) oxygen surface exchange coefficients.

The activation enthalpies of diffusion are relatively similar, being ΔH_{D^*} = (1.35 ± 0.06) eV for STF50 and ΔH_{D^*} = (1.47 ± 0.07) eV for SF. The data obtained for k^* show much more scatter, and the values for SF and STF50 compositions are relatively similar. The associated activation enthalpies, however, differ significantly, with ΔH_{k^*} = (0.81 ± 0.08) eV for STF50 and ΔH_{D^*} = (1.53 ± 0.23) eV for SF.

5 Discussion

5.1 Diffusion

In Fig. 5 we plot for T = 873 K our oxygen diffusion coefficients together with data taken from the literature.[27,43,49,51–54] Surprisingly, one observes no maximum in D^* but a monotonic increase with Fe concentration, albeit with some scatter at high levels of Fe. In contrast, characteristic acceptor-doped oxides, such as perovskite-structured gallates[85,86] or fluorite-structured ceria,[87,88] all display a maximum in ion conductivity as a function of acceptor-dopant level.[89,90] At first sight, this absence of a maximum implies that point-defect interactions involving oxygen vacancies are negligible in the STF system: substituting Fe for Ti thus appears to introduce oxygen vacancies into the system, but Fe itself does not trap the vacancies nor does it influence their rate of migration. As we will see, closer inspections indicate more complicated behaviour.

Let us note, first, that there is a gap in experimental data (and the defect-chemical predictions) for the intermediate regime, $10^{19.7} \leq$ [Fe]/cm^{-3} $\leq 10^{21.2}$, *i.e.*, from below 1% to *ca.* 10% site fraction of Fe. It is conceivable that defect interactions make themselves explicitly evident in this intermediate region. Second, let us examine the behaviour quantitatively. Although the behaviour of D^* in Fig. 5 follows that of $[V_O^{\bullet\bullet}]$ in Fig. 1(a) predicted by Models I–III, $[V_O^{\bullet\bullet}]$ increases by 4–4.5 orders of magnitude over the range of [Fe] shown, whereas D^* only increases by *ca.* 3.5 orders

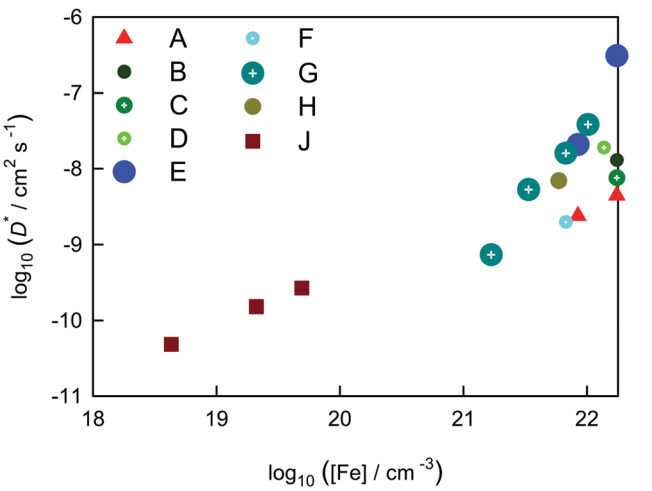

Fig. 5 Oxygen tracer diffusion coefficients as a function of Fe concentration for T = 873 K. Symbols refer to experimental data, extrapolated where necessary (squares, from single crystals; circles, from ceramics, and triangles, from thin films): (A) this work; (B) Yoo and Jacobson;[51] (C) Wang *et al.*;[55] (D) Mashkina *et al.*;[52] (E) Rothschild *et al.*;[49] (F) Fagg *et al.*;[53] (G) Steinsvik *et al.*;[43] (H) Argirusis *et al.*;[54] (J) Claus *et al.*[27]

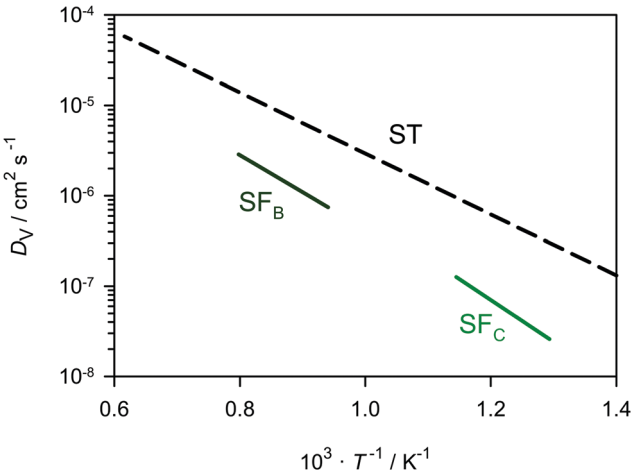

Fig. 6 Comparison of D_V values for the two end-members: ST ($\Delta H_{mig,V}$ = 0.67 eV)[30] and SF_B[51] and SF_C[55] ($\Delta H_{mig,V}$ = 0.81 eV describes both datasets together).

of magnitude. From eqn (9) we conclude that, if the predictions of the models are correct, the isothermal value of $f_V^* D_V$ cannot be constant across the entire system. That is, Fe substitution evidently changes $f_V^* D_V$. Indeed, in Fig. 6 we see that D_V for the end-members differ by *ca.* one order of magnitude. Although we cannot rule out that both f_V^* and D_V show complex behaviour for compositions between the end-members, the simplest interpretation suggests that f_V^* is constant and D_V varies smoothly in some manner between the two extremes.

The data shown in Fig. 5, it is emphasised, was converted in many cases from ionic conductivities with the standard value[78] for f_V^* and was extrapolated, where necessary, from data obtained at higher/lower temperatures. This extrapolation necessarily introduces larger uncertainties into the data plotted in Fig. 5. It is also emphasised that, although all data refer to T = 873 K, they do not refer to the same oxygen activity. Some datasets refer to high oxygen activities ($1 \ll aO_2 \ll 10^{-2}$), namely tracer data obtained for single crystal samples[27] and for STF35 ceramics;§[54] chemical diffusion data for SF ceramics;[51] data converted from ionic conductivities measured for STF40 ceramics.[53] In contrast, all other data converted from ionic conductivities measured for various STF ceramics,[43] STF80 ceramics,[52] and STF50 and SF ceramics[49] were obtained from the intermediate plateau in conductivity *versus* oxygen activity plots and refer therefore to more reducing conditions ($aO_2 < 10^{-6}$). Whether this explains the scatter in the data for high c_{Fe} shown in Fig. 5 is unclear; the data obtained at lower oxygen activities (E and G) are consistently higher than those obtained under more oxidising conditions (B, C and F).

D^* measured for our thin-film samples is considerably lower than values obtained for ceramics, with the exception of data obtained by Fagg *et al.*[53] We consider two possible reasons for this behaviour. First, it is possible that microstructural differences are responsible. The thin films consisted of small columnar grains ($d_{gr} \sim 10^2$ nm) and with isotope diffusion occurring perpendicular to the GBs (in the plane of the film), and penetrating $\sim 10^5$ nm, the diffusing species crossed a huge number of grain boundaries. Compared with ceramics (*e.g.*, STF35[54]), in which the isotope profiles extended hundred of micrometers and the grain size, though not given, was probably of the order of micrometers, the present case of thin films is characterised by the number of grain boundaries that have to be crossed being higher by one, if not two, orders of magnitude. As to why the GBs hinder oxygen transport, we can rule out space-charge layers that are depleted of oxygen vacancies: such layers, though present at grain boundaries in weakly doped ST ceramics and bicrystals,[91–100] are not evident at GBs in ceramics with $y > 0.07$.[91,101,102] Space-charge layers may be present in these concentrated solid solutions, but they may display complex behaviour, *e.g.*, co-accumulation of dopants and vacancies.[103,104] Consequently, the origin of the resistance, in this case of STF thin films, would appear to be purely structural, the intrinsic resistance arising from the strong structural perturbation of the perovskite structure at GBs.

An alternative, and more likely, explanation is that defect interactions are important. Specifically, *A*-site cation vacancies have been predicted to increase the activation enthalpy of oxygen-vacancy migration in an ABO_3 perovskite,[105] leading thus to lower oxygen diffusivities. In this way, the different method of preparation for the thin-film samples results in a lower oxygen diffusivity. PLD, namely, may produce perovskite films with high, non-equilibrium amounts of vacancies on one or even both cation sublattices.[106,107] In this regard, the data of Fagg *et al.*[53] were obtained for a nominally *A*-site deficient composition, $Sr_{0.97}Ti_{0.6}Fe_{0.4}O_{3-\delta}$.

The activation enthalpies of oxygen tracer diffusion are plotted in Fig. 7. We consider the weakly doped compositions (Model I, [Fe] $< 10^{20}$ cm^{-3}) and the concentrated solutions (Models II and III, [Fe] $> 10^{21}$ cm^{-3}) separately. For the former, we see a small increase in ΔH_{D^*} with increasing [Fe]. Using the data for $\Delta H_{gen,V}$ from Fig. 1(b), one obtains, according to eqn (10), values for the migration enthalpy of oxygen vacancies in Fe-doped $SrTiO_3$ of $\Delta H_{mig,V}$ = 0.76–0.90 eV. Although these values agree well with $\Delta H_{mig,V}$ = 0.86 eV reported by Denk *et al.*,[73] they are significantly higher than the value of $\Delta H_{mig,V}$ = 0.6 eV obtained for nominally un-doped $SrTiO_3$.[20,24,30,31,33,108] The difference arises from Fe, as an acceptor dopant, strongly affecting the behaviour of oxygen vacancies. Specifically, Fe increases the activation enthalpy for vacancy migration in the vicinity of the dopant, and it also tends to trap a vacancy in its vicinity. Together, these two effects lead to an increase in the effective activation enthalpy of migration.[32] The value of 0.86 eV derived by Denk *et al.*[73] thus implicitly includes the effect of defect interactions on the vacancy mobility.

The behaviour seen in Fig. 7 for the concentrated solid solutions is unclear, even if our two data points (A) are ignored. Again, there are differences between data obtained under oxidising and reducing conditions: the latter (E and G) are lower and indicate a decrease with increasing [Fe], whilst the former (B, C, D, F and H) are roughly constant at just below 1 eV. Defect models II and III both indicate $\Delta H_{gen,V}$ = 0.1–0.2 eV at

§ Data reported in the original paper[54] is incorrect. Corresponding author of that paper kindly provided correct data.

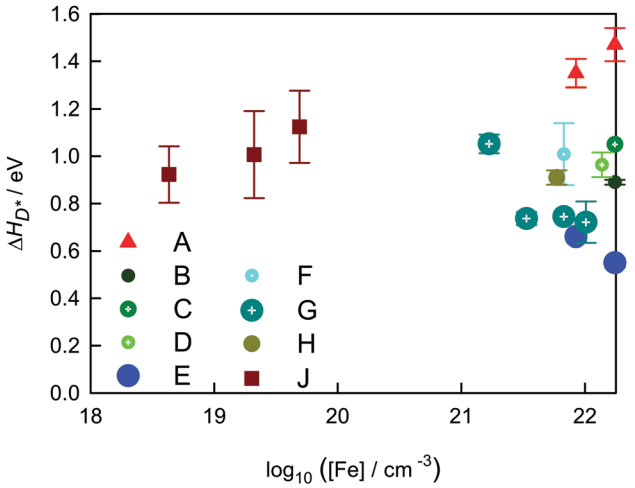

Fig. 7 Activation enthalpies of oxygen tracer diffusion as a function of Fe concentration for T = 873 K. Symbols refer to experimental data (squares, from single crystals; circles, from ceramics, and triangles, from thin films): (A) this work; (B) Yoo and Jacobson;[51] (C) Wang *et al.*;[55] (D) Mashkina *et al.*;[52] (E) Rothschild *et al.*;[49] (F) Fagg *et al.*;[53] (G) Steinsvik *et al.*;[54] (H) Argirusis *et al.*;[54] (J) Claus *et al.*[27]

high oxygen activities; under reducing conditions, $\Delta H_{gen,V}$ is expected to go to zero, because Fe is present exclusively as Fe^{3+}. Thus the data at high oxygen activities are generally consistent with the defect models but the scatter and the lack of data from Models II and III prevents further analysis.

5.2 Oxygen surface exchange

5.2.1 Introductory comments. There are several reasons why we know so much more about diffusion in the bulk than oxygen exchange at the surface. First, it is because a measured surface exchange coefficient refers to the overall rate of a multi-step reaction: it is a macroscopic measure of a consecutive series of microscopic processes. And while specific processes certainly have to be involved—the adsorption and the dissociation of oxygen molecules, the transfer of charge between (various possible) oxygen adsorbates and the oxide substrate, and the incorporation of an oxygen adatom into a vacant oxygen site—the particular sequence of steps and the particular step that is rate limiting are unknown. Second, it is because the composition of a surface may differ significantly from that of the bulk phase,[57,109–113] not only with regard to matrix species but also with regard to contaminants. Generally, the structure and the composition, and thus the reactivity, of a surface will, conceivably, be very sensitive to preparation procedures. Third, it is because a surface, as an extended defect, does not have to obey local neutrality.[114] A surface may be electrostatically charged, with global neutrality being satisfied by an adjacent space-charge zone that extends many nanometers into the bulk, even in a concentrated solution.[103,104] Both charged surface and compensating space-charge zone will be characterised by defect concentrations that differ hugely from the bulk values, with the concentrations of defects at the very surface (the reaction partners of molecules in the gas phase) not being related in any simple manner to defect concentrations in the bulk phase. This point has not been taken into account properly in any study to date, especially those on acceptor-doped $SrTiO_3$,[34,36,38,40] for which a surface space-charge layer has been detected.[29–31,115] Previous analyses and conclusions need, therefore, to be re-evaluated. In short, the complexities one faces in studying and understanding mass transport in the solid state are multiplied at a surface.

5.2.2 Literature comparison. Merkle and Maier[37] examined the rate of oxygen incorporation into Fe-doped $SrTiO_3$ (an electron-poor material) and $SrTi_{0.7}Fe_{0.3}O_3$ (an electron-rich material). They found that the surface reaction rate was higher for the electron-rich material, with a significantly lower activation enthalpy. On this basis they proposed that different reaction mechanisms are operative for electron-poor materials and electron-rich materials.

In Fig. 8 and 9 we show the isothermal variation in k^* at T = 873 K and the variation in the activation enthalpy of k^* across the STF system (comparing our data with values from the literature[34,47,51,54]). In neither plot do we see a sudden jump in behaviour that would be indicative of different reaction mechanisms. Rather we see, if we start at Fe-doped $SrTiO_3$ and extrapolate up to higher [Fe], that $\log_{10} k^*$ increases almost linearly with $\log_{10}$ [Fe]. In other words, if many STF compositions are considered (rather than just two) the data argues strongly for one common mechanism of oxygen surface exchange for the entire STF system.

In constructing Fig. 8 and 9 we have not only taken directly data from tracer studies (k^*) but we have also converted data from chemical (k^δ) and electrical (k^q) studies. It has been proposed[116] that (at least for electron-poor materials) k^* and k^δ are not simply related to one another through the thermodynamic factor because chemical and tracer incorporation of

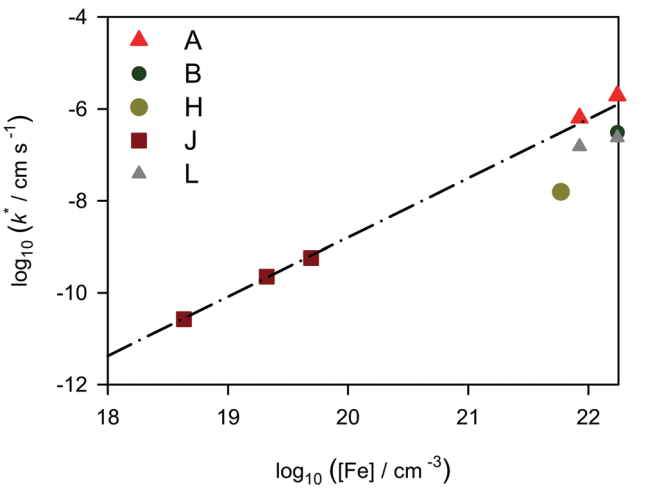

Fig. 8 Oxygen tracer surface exchange coefficients as a function of Fe concentration for T = 873 K. Symbols refer to experimental data, extrapolated where necessary (squares, from single crystals; circles, from ceramics, and triangles, from thin films): (A) this work; (B) Yoo and Jacobson;[51] (H) Argirusis *et al.*;[54] (J) Leonhardt *et al.*;[34] (L) Jung and Tuller.[47] Dashed-dotted line is a guide to the eye.

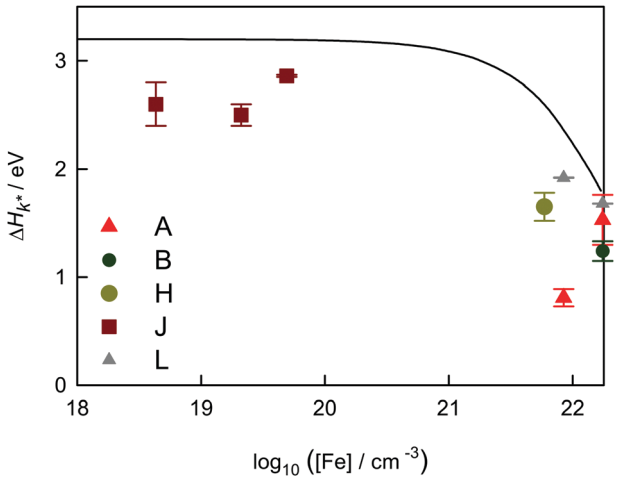

Fig. 9 Activation enthalpies of oxygen tracer surface exchange as a function of Fe concentration for T = 873 K. Symbols refer to experimental data (squares, from single crystals; circles, from ceramics, and triangles, from thin films): (A) this work; (B) Yoo and Jacobson;[51] (G) Argirusis *et al.*;[54] (J) Leonhardt *et al.*;[34] (L) Jung and Tuller.[47] Black line is the variation in the bandgap according to Rothschild *et al.*[49]

molecular oxygen may occur by different mechanisms, tracer incorporation not formally requiring electrons. This proposal can be discounted, however, for it requires any natural fluctuation away from the equilibrium state to return to the equilibrium state by a different mechanism, thus violating the principle of microscopic reversibility. Hence as long as chemical incorporation is performed with small driving forces, such that the reaction rate can be linearised,[117,118] there should be no difference between k^* and k^δ.

We have also restricted the data plotted in Fig. 8 and 9 to data obtained by analysing the oxygen flux into the solid, rather than the rate of reaction in the gas phase.[56] The former specifically assumes that the kinetics are first order, although this is not necessarily the case.[119] Gas-phase data do not suffer from this restriction.

What, then, is the common mechanism of surface exchange? (We emphasise that the conclusion of a single mechanism is the simplest possible interpretation of Fig. 8 and 9. More complicated variations are, of course, conceivable.) We refrain here from proposing a specific mechanism (we do not have sufficient information to do so), but we do identify a probable rate-determining species. Relaxation experiments under UV illumination by Merkle *et al.*[35,36] unambiguously demonstrate that conduction-band electrons are required for oxygen incorporation into Fe-doped $SrTiO_3$. Jung and Tuller,[47] having examined the variation in surface reaction rate across the STF system, came to the same conclusion. And De Souza[119] previously argued that a mechanistic scheme with conduction-band electrons in the rate-determining step was consistent with the measured dependence of k^* on aO_2 for diverse acceptor-doped perovskite and fluorite oxides. In Fig. 9 we see that across the entire STF system ΔH_{k^*} broadly follows the variation in the bandgap,[49] as predicted.[119] The surprising point, perhaps, is that there is any correlation at all with the bulk value of the bandgap, given that the bandgap at the surface may differ substantially from the value in the bulk.[58] Nevertheless, the main conclusion here is that minority species—electrons in the conduction band—are required in STF oxides for oxygen surface exchange to occur.

Exactly how or why do conduction-band electrons determine the rate of surface exchange? We suggest two explanations, both of which, in line with previous studies,[36,58] rely on the electronic energy levels of the oxygen adsorbates on the oxide surface lying close to or above the conduction-band edge. Thus, in the first explanation the reaction rate is limited by the sheer low number of electrons in the conduction band of an acceptor-doped oxide under oxidising conditions. Alternatively, in the second explanation an additional limitation is provided by activation barriers that hinder the transfer of electrons from the conduction band to the adsorbate levels. Both these possibilities are illustrated schematically in Fig. 10.

In this regard three further points are important. First, these two explanations are not restricted to oxides with a band-gap: electron transfer can be rate limiting, even for oxides with half-filled bands, if the adsorbate levels lie well above the Fermi level and/or if there are activation barriers to charge transfer. Second, Fig. 10 shows the case of a neutral surface (*i.e.*, without band bending). Positively charged interfaces in $SrTiO_3$ are known to display a considerable resistance to mass transport because of the strong depletion of oxygen vacancies in the attendant space-charge zone.[91–100] In the case of a surface, however, the presence of a positively charged surface with a negative space-charge layer may be, in fact, overall beneficial. Although oxygen vacancies will be depleted in the space-charge zone, giving rise to an additional resistance that decreases the effective magnitude of k^*,[29] the concentration of electrons at the very surface will be drastically enhanced, thereby increasing k^*. Third, the explanations are not consistent with DFT calculations performed by Staykov *et al.*[41] for the SrO-terminated surface of $SrTiO_3$, but this may be due to issues intrinsic to DFT calculations. Staykov *et al.*[41] concluded that oxygen vacancies in the SrO-terminated surface are critical reaction species because they provide access to the catalytically active TiO_6 manifold of the perovskite. These DFT calculations refer, however, to T = 0 K,

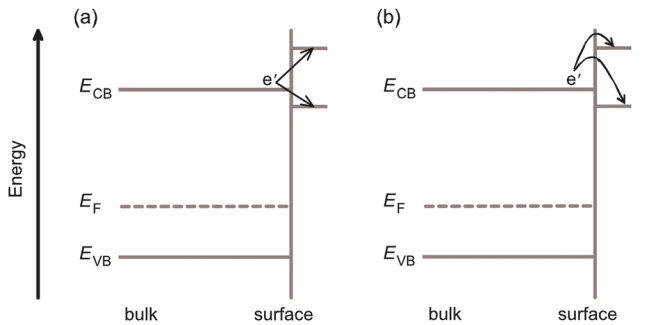

Fig. 10 Schematic diagram of the electronic band structure of an acceptor-doped oxide at the surface, showing the possible energy levels of oxygen adsorbates to which conduction-band electrons may be transferred: without (a) and with (b) activation barriers to electron transfer. E_{CB}, energy of the conduction-band edge; E_{VB}, energy of the valence-band edge; E_F, Fermi level. Based on ref. 36 and 58.

i.e., to a temperature at which the conduction band is entirely empty of electrons. Furthermore, it is debatable whether DFT calculations of the surface reaction[41,120–125] may find electron transfer as the rate-determining step, as such calculations refer to the electronic ground state of the system. It is unclear, therefore, whether Staykov *et al.*[41] have identified the correct rate-determining step and reaction mechanism.

To reach conclusions about k^* for the entire STF system, we have made use of Fig. 8 and 9 and the results obtained for one end-member (ST). One can continue this approach by extending a further tie-line, from $SrFeO_3$ to $LaFeO_3$. Results obtained here could be extended to (La,Sr)FeO_3 materials,[117,118,126,127] and, of course, vice versa. The important point that needs to be considered is the potential role that minority charge carriers (in semiconductors) and electrons well above the Fermi level (in metallic conductors) play in the exchange process.

6 Concluding remarks

We critically examined oxygen diffusion and surface exchange in the $SrTi_{1-y}Fe_yO_{3-\delta}$ perovskite oxides. The following points emerged from our study:

• Oxygen diffusion occurs by a vacancy migration across the entire STF series.

• The oxygen diffusivity increases continuously as a function of Fe concentration.

• Oxygen surface exchange occurs apparently by one single mechanism for electron-poor and electron-rich STF materials.

• The energy levels of oxygen adsorbates at the oxide surface, relative to the energy of the conduction-band edge, are proposed to play a key role.

Acknowledgements

VM and RADS acknowledge funding from the German Science Foundation (DFG) within the collaborative research centre, SFB 917 ''Nanoswitches''. WCJ, SRB and HLT acknowledge the US-Department of Energy—Basic Energy Sciences, Grant No. DE-SC0002633, for financial support. Discussions with D. N. Mueller, A. Klein and D. S. Mebane are gratefully acknowledged. T. Norby and C. Argirusis are thanked for providing data.

References

1 H. J. M. Bouwmeester, H. Kruidhof and A. J. Burggraaf, *Solid State Ionics*, 1994, **72**(part 2), 185–194.
2 B. C. H. Steele, *Solid State Ionics*, 1995, **75**, 157–165.
3 J. A. Kilner, R. A. De Souza and I. C. Fullarton, *Solid State Ionics*, 1996, **86–88**, 703–709.
4 S. B. Adler, *Chem. Rev.*, 2004, **104**, 4791–4844.
5 E. Tsipis and V. Kharton, *J. Solid State Electrochem.*, 2008, **12**, 1039–1060.
6 J. Maier, *Solid State Ionics*, 1998, **112**, 197–228.
7 S. Kim, Y. Yang, A. Jacobson and B. Abeles, *Solid State Ionics*, 1998, **106**, 189–195.
8 Y. Choi, D. S. Mebane, J.-H. Wang and M. Liu, *Top. Catal.*, 2007, **46**, 386–401.
9 W. C. Chueh and S. M. Haile, *Annu. Rev. Chem. Biomol. Eng.*, 2012, **3**, 313–341.
10 Z. Shao, W. Yang, Y. Cong, H. Dong, J. Tong and G. Xiong, *J. Membr. Sci.*, 2000, **172**, 177–188.
11 Z. Shao and S. M. Haile, *Nature*, 2004, **431**, 170–173.
12 E. Bucher, A. Egger, P. Ried, W. Sitte and P. Holtappels, *Solid State Ionics*, 2008, **179**, 1032–1035.
13 L. Wang, R. Merkle, J. Maier, T. Acartürk and U. Starke, *Appl. Phys. Lett.*, 2009, **94**, 071908.
14 S. Švarcová, K. Wiik, J. Tolchard, H. J. Bouwmeester and T. Grande, *Solid State Ionics*, 2008, **178**, 1787–1791.
15 D. N. Mueller, R. A. De Souza, J. Brendt, D. Samuelis and M. Martin, *J. Mater. Chem.*, 2009, **19**, 1960–1963.
16 D. N. Mueller, R. A. De Souza, T. E. Weirich, D. Roehrens, J. Mayer and M. Martin, *Phys. Chem. Chem. Phys.*, 2010, **12**, 10320–10328.
17 D. N. Mueller, R. A. De Souza, H.-I. Yoo and M. Martin, *Chem. Mater.*, 2012, **24**, 269–274.
18 R. A. De Souza, J. Fleig, R. Merkle and J. Maier, *Z. Metallkd.*, 2003, **94**, 218–225.
19 A. E. Paladino, L. G. Rubin and J. S. Waugh, *J. Phys. Chem. Solids*, 1965, **26**, 391–397.
20 D. B. Schwarz and H. U. Anderson, *J. Electrochem. Soc.*, 1975, **122**, 707–710.
21 J. C. Amante, J. D. Cawley, J. Kim and T. R. Lemberger, Point Defects and Related Properties of Ceramics, *Ceram. Trans.*, Westerville, Ohio, 1991, pp. 303–312.
22 A. Müller and K. Härdtl, *Appl. Phys. A: Mater. Sci. Process.*, 1989, **49**, 75–82.
23 P. Pasierb, S. Komornicki and M. Rekas, *J. Phys. Chem. Solids*, 1999, **60**, 1835–1844.
24 A. Hackmann and O. Kanert, *Radiat. Eff. Defects Solids*, 1991, **119–121**, 651–656.
25 T. Bieger, J. Maier and R. Waser, *Solid State Ionics*, 1992, **53–56**(part 1), 578–582.
26 I. Denk, F. Noll and J. Maier, *J. Am. Ceram. Soc.*, 1997, **80**, 279–285.
27 J. Claus, M. Leonhardt and J. Maier, *J. Phys. Chem. Solids*, 2000, **61**, 1199–1207.
28 R. A. De Souza, J. Zehnpfenning, M. Martin and J. Maier, *Solid State Ionics*, 2005, **176**, 1465–1471.
29 R. A. De Souza and M. Martin, *Phys. Chem. Chem. Phys.*, 2008, **10**, 2356–2367.
30 R. A. De Souza, V. Metlenko, D. Park and T. E. Weirich, *Phys. Rev. B: Condens. Matter Mater. Phys.*, 2012, **85**, 174109.
31 V. Metlenko, A. Ramadan, F. Gunkel, H. Du, H. Schraknepper, S. Hoffmann-Eifert, R. Dittmann, R. Waser and R. A. De Souza, *Nanoscale*, 2014, **6**, 12864–12876.
32 M. Schie, R. Waser and R. A. De Souza, *J. Phys. Chem. C*, 2014, **118**, 15185–15192.
33 S. P. Waldow and R. A. De Souza, *ACS Appl. Mater. Interfaces*, 2016, **8**, 12246–12256.
34 M. Leonhardt, R. A. De Souza, J. Claus and J. Maier, *J. Electrochem. Soc.*, 2002, **149**, J19–J26.

35 R. Merkle, R. A. De Souza and J. Maier, *Angew. Chem., Int. Ed.*, 2001, **40**, 2126–2129.
36 R. Merkle and J. Maier, *Phys. Chem. Chem. Phys.*, 2002, **4**, 4140–4148.
37 R. Merkle and J. Maier, *Top. Catal.*, 2006, **38**, 141–145.
38 S. F. Wagner, C. Warnke, W. Menesklou, C. Argirusis, T. Damjanović, G. Borchardt and E. Ivers-Tiffée, *Solid State Ionics*, 2006, **177**, 1607–1612.
39 C. Argirusis, S. Wagner, W. Menesklou, C. Warnke, T. Damjanović, G. Borchardt and E. Ivers-Tiffée, *Phys. Chem. Chem. Phys.*, 2005, **7**, 3523–3525.
40 K. Kerman, C. Ko and S. Ramanathan, *Phys. Chem. Chem. Phys.*, 2012, **14**, 11953–11960.
41 A. Staykov, H. Téllez, T. Akbay, J. Druce, T. Ishihara and J. Kilner, *Chem. Mater.*, 2015, **27**, 8273–8281.
42 L. Brixner, *Mater. Res. Bull.*, 1968, **3**, 299–308.
43 S. Steinsvik, T. Norby and P. Kofstad, *Proc. Electroceramics IV*, Aachen, Germany, 1994, pp. 691–696.
44 W. Menesklou, H.-J. Schreiner, K. H. Härdtl and E. Ivers-Tiffée, *Sens. Actuators, B*, 1999, **59**, 184–189.
45 J. Mizusaki, M. Okayasu, S. Yamauchi and K. Fueki, *J. Solid State Chem.*, 1992, **99**, 166–172.
46 W. Jung and H. L. Tuller, *J. Electrochem. Soc.*, 2008, **155**, B1194–B1201.
47 W. Jung and H. L. Tuller, *Adv. Energy Mater.*, 2011, **1**, 1184–1191.
48 S. Steinsvik, R. Bugge, J. Gjønnes, J. Taftø and T. Norby, *J. Phys. Chem. Solids*, 1997, **58**, 969–976.
49 A. Rothschild, W. Menesklou, H. L. Tuller and E. Ivers-Tiffée, *Chem. Mater.*, 2006, **18**, 3651–3659.
50 S. Steinsvik, Y. Larring and T. Norby, *Solid State Ionics*, 2001, **143**, 103–116.
51 J. Yoo and A. J. Jacobson, *Mat. Res. Soc. Symp. Proc.*, 2003, 756, EE3.10.1.
52 E. Mashkina, A. Magerl, J. Ollivier, M. Göbbels and F. Seifert, *Phys. Rev. B: Condens. Matter Mater. Phys.*, 2006, **74**, 214106.
53 D. Fagg, V. Kharton, A. Kovalevsky, A. Viskup, E. Naumovich and J. Frade, *J. Eur. Ceram. Soc.*, 2001, **21**, 1831–1835.
54 C. Argirusis, F. Jomard, S. F. Wagner, W. Menesklou and E. Ivers-Tiffée, *Solid State Ionics*, 2011, **192**, 9–11.
55 L. Wang, R. Merkle and J. Maier, *J. Electrochem. Soc.*, 2010, **157**, B1802–B1808.
56 C.-Y. Yoo and H. J. M. Bouwmeester, *Phys. Chem. Chem. Phys.*, 2012, **14**, 11759–11765.
57 W. Jung and H. L. Tuller, *Energy Environ. Sci.*, 2012, **5**, 5370–5378.
58 Y. Chen, W. Jung, Z. Cai, J. J. Kim, H. L. Tuller and B. Yildiz, *Energy Environ. Sci.*, 2012, **5**, 7979–7988.
59 A. Nenning, E. Navickas, P. Velicsanyi, A. K. Opitz, H. Hutter and J. Fleig, *Solid State Ionics*, 2015, **273**, 25–29.
60 R. A. De Souza and M. Martin, *MRS Bull.*, 2009, **34**, 907–914.
61 P. Fielitz and G. Borchardt, *Solid State Ionics*, 2001, **144**, 71–80.
62 R. A. De Souza and R. J. Chater, *Solid State Ionics*, 2005, **176**, 1915–1920.
63 J. A. Kilner, S. J. Skinner and H. H. Brongersma, *J. Solid State Electrochem.*, 2011, **15**, 861–876.
64 T. Norby, *J. Mater. Chem.*, 2001, **11**, 11–18.
65 T. Norby, *J. Korean Ceram. Soc.*, 2010, **47**, 19–25.
66 N.-H. Chan, R. K. Sharma and D. M. Smyth, *J. Electrochem. Soc.*, 1981, **128**, 1762–1769.
67 U. Balachandran and N. Eror, *J. Solid State Chem.*, 1981, **39**, 351–359.
68 G. M. Choi, H. L. Tuller and D. Goldschmidt, *Phys. Rev. B: Condens. Matter Mater. Phys.*, 1986, **34**, 6972–6979.
69 G. M. Choi and H. L. Tuller, *J. Am. Ceram. Soc.*, 1988, **71**, 201–205.
70 R. Waser, *J. Am. Ceram. Soc.*, 1991, **74**, 1934–1940.
71 R. Waser, T. Bieger and J. Maier, *Solid State Commun.*, 1990, **76**, 1077–1081.
72 R. Moos and K. H. Härdtl, *J. Am. Ceram. Soc.*, 1997, **80**, 2549–2562.
73 I. Denk, W. Münch and J. Maier, *J. Am. Ceram. Soc.*, 1995, **78**, 3265–3272.
74 C.-J. Shin, H.-I. Yoo and C.-E. Lee, *Solid State Ionics*, 2007, **178**, 1081–1087.
75 C.-J. Shin and H.-I. Yoo, *Solid State Ionics*, 2007, **178**, 1089–1094.
76 R. A. De Souza, *Adv. Funct. Mater.*, 2015, **25**, 6326–6342.
77 T. Shi, Y. Chen and X. Guo, *Prog. Mater. Sci.*, 2016, **80**, 77–132.
78 T. Ishigaki, S. Yamauchi, K. Kishio, J. Mizusaki and K. Fueki, *J. Solid State Chem.*, 1988, **73**, 179–187.
79 J. Crawford and P. Jacobs, *J. Solid State Chem.*, 1999, **144**, 423–429.
80 A. Samanta, W. E and S. B. Zhang, *Phys. Rev. B: Condens. Matter Mater. Phys.*, 2012, **86**, 195107.
81 M. Kuhn, J. J. Kim, S. R. Bishop and H. L. Tuller, *Chem. Mater.*, 2013, **25**, 2970–2975.
82 R. A. De Souza and J. A. Kilner, *Solid State Ionics*, 1998, **106**, 175–187.
83 M. Burriel, G. Garcia, J. Santiso, J. A. Kilner, R. J. Chater and S. J. Skinner, *J. Mater. Chem.*, 2008, **18**, 416–422.
84 J. Crank, *The Mathematics of Diffusion*, Oxford University Press, Oxford, 2nd edn, 1975.
85 K. Huang, R. S. Tichy and J. B. Goodenough, *J. Am. Ceram. Soc.*, 1998, **81**, 2565–2575.
86 A. Petric and P. Huang, *Solid State Ionics*, 1996, **92**, 113–117.
87 D. Y. Wang, D. Park, J. Griffith and A. Nowick, *Solid State Ionics*, 1981, **2**, 95–105.
88 J. Faber, C. Geoffroy, A. Roux, A. Sylvestre and P. Abélard, *Appl. Phys. A: Mater. Sci. Process.*, 1989, **49**, 225–232.
89 H. L. Tuller, *J. Phys. Chem. Solids*, 1994, **55**, 1393–1404.
90 J. Kilner, *Solid State Ionics*, 2000, **129**, 13–23.
91 R. A. De Souza, *Phys. Chem. Chem. Phys.*, 2009, **11**, 9939–9969.
92 I. Denk, J. Claus and J. Maier, *J. Electrochem. Soc.*, 1997, **144**, 3526–3536.
93 R. Hagenbeck and R. Waser, *J. Appl. Phys.*, 1998, **83**, 2083–2092.
94 S. Rodewald, J. Fleig and J. Maier, *J. Am. Ceram. Soc.*, 2001, **84**, 521–530.
95 R. Waser and R. Hagenbeck, *Acta Mater.*, 2000, **48**, 797–825.

96 P. Lupetin, G. Gregori and J. Maier, *Angew. Chem., Int. Ed.*, 2010, **49**, 10123–10126.
97 R. A. De Souza, J. Fleig, J. Maier, O. Kienzle, Z. Zhang, W. Sigle and M. Rühle, *J. Am. Ceram. Soc.*, 2003, **86**, 922–928.
98 R. A. De Souza, J. Fleig, J. Maier, Z. Zhang, W. Sigle and M. Rühle, *J. Appl. Phys.*, 2005, **97**, 053502.
99 Z. Zhang, W. Sigle, R. A. De Souza, W. Kurtz, J. Maier and M. Rühle, *Acta Mater.*, 2005, **53**, 5007–5015.
100 X. Guo, Z. Zhang, W. Sigle, E. Wachsman and R. Waser, *Appl. Phys. Lett.*, 2005, **87**, 162105.
101 J. R. Jurado, M. T. Colomer and J. R. Frade, *J. Am. Ceram. Soc.*, 2000, **83**, 2715–2720.
102 J. R. Jurado, M. T. Colomer and J. R. Frade, *Solid State Ionics*, 2001, **143**, 251–257.
103 D. S. Mebane, *Comput. Mater. Sci.*, 2015, **103**, 231–236.
104 D. S. Mebane and R. A. De Souza, *Energy Environ. Sci.*, 2015, **8**, 2935–2940.
105 A. Walsh, C. R. A. Catlow, A. G. H. Smith, A. A. Sokol and S. M. Woodley, *Phys. Rev. B: Condens. Matter Mater. Phys.*, 2011, **83**, 220301.
106 D. J. Keeble, S. Wicklein, R. Dittmann, L. Ravelli, R. A. Mackie and W. Egger, *Phys. Rev. Lett.*, 2010, **105**, 226102.
107 H. Schraknepper, C. Baumer, R. Dittmann and R. A. De Souza, *Phys. Chem. Chem. Phys.*, 2015, **17**, 1060–1069.
108 F. Cordero, *Phys. Rev. B: Condens. Matter Mater. Phys.*, 2007, **76**, 172106.
109 G. M. Rupp, H. Tellez, J. Druce, A. Limbeck, T. Ishihara, J. Kilner and J. Fleig, *J. Mater. Chem. A*, 2015, **3**, 22759–22769.
110 J. Druce, H. Tellez, M. Burriel, M. D. Sharp, L. J. Fawcett, S. N. Cook, D. S. McPhail, T. Ishihara, H. H. Brongersma and J. A. Kilner, *Energy Environ. Sci.*, 2014, **7**, 3593–3599.
111 J. Druce, T. Ishihara and J. Kilner, *Solid State Ionics*, 2014, **262**, 893–896.
112 K. V. Hansen, K. Norrman and M. Mogensen, *Surf. Interface Anal.*, 2006, **38**, 911–916.
113 M. J. Pietrowski, R. A. De Souza, M. Fartmann, R. ter Veen and M. Martin, *Fuel Cells*, 2013, **13**, 673–681.
114 J. Maier, *Physical Chemistry of Ionic Materials: Ions and Electrons in Solids*, J. Wiley & Sons, Chichester, 2004.
115 H. Schraknepper and R. A. De Souza, *J. Appl. Phys.*, 2016, **119**, 064903.
116 J. Maier, *Solid State Ionics*, 2000, **135**, 575–588.
117 S. Adler, X. Chen and J. Wilson, *J. Catal.*, 2007, **245**, 91–109.
118 M. Mosleh, M. Søgaard and P. V. Hendriksen, *J. Electrochem. Soc.*, 2009, **156**, B441–B457.
119 R. A. De Souza, *Phys. Chem. Chem. Phys.*, 2006, **8**, 890–897.
120 Y. Choi, D. S. Mebane, M. C. Lin and M. Liu, *Chem. Mater.*, 2007, **19**, 1690–1699.
121 Y. Choi, M. E. Lynch, M. C. Lin and M. Liu, *J. Phys. Chem. C*, 2009, **113**, 7290–7297.
122 Y. A. Mastrikov, R. Merkle, E. Heifets, E. A. Kotomin and J. Maier, *J. Phys. Chem. C*, 2010, **114**, 3017–3027.
123 G. Pilania and R. Ramprasad, *Surf. Sci.*, 2010, **604**, 1889–1893.
124 H. Guhl, W. Miller and K. Reuter, *Surf. Sci.*, 2010, **604**, 372–376.
125 V. Alexandrov, S. Piskunov, Y. F. Zhukovskii, E. A. Kotomin and J. Maier, *Integr. Ferroelectr.*, 2011, **123**, 10–17.
126 N. H. Perry, D. Pergolesi, S. R. Bishop and H. L. Tuller, *Solid State Ionics*, 2015, **273**, 18–24.
127 D. N. Mueller, M. L. Machala, H. Bluhm and W. C. Chueh, *Nat. Commun.*, 2015, **6**, 6097.